Dual-band Optical Filters Using Integrated Multimode Bragg Gratings

Jonathan Cauchon and Wei Shi

Centre d'optique, photonique et laser (COPL), Département de génie électrique et de génie informatique, Université Laval, 2375 rue de la Terrasse, Québec (Qc), Canada, G1V 0A6.

wei.shi@gel.ulaval.ca

Abstract: We demonstrate a multimode integrated Bragg grating allowing dual-band filtering in the 1.5-1.6 μm region. Bandwidths of 4.4 and 7.5 nm and a band separation of 42 nm are achieved.

OCIS codes: (130.7408) Wavelength filtering devices, (350.2770) Gratings, (230.1480) Bragg reflectors, (130.3120) Integrated optics devices.

1. Introduction

Optical networks provide the physical foundation for high-speed data exchange through optical fibers. With the ever-increasing volume of data traffic, data centers and service providers need to keep up with novel modulating and multiplexing devices. The silicon-on-insulator platform has proven to be promising in that regard, due to its compatibility with established CMOS manufacturing processes, small footprint, and remarkably low energy consumption. Along with the integrated-optics paradigm comes the need for various building blocks of such systems. Passive filters are among those devices crucial for the evolution of optical networks. Single-band filtering is typically achieved using either microring-based or grating-based devices. In the same way, dual-band optical filters find use in telecommunications, namely for dual-band WDM [1]. Dual-band operation has been demonstrated using multimode microdisk resonators [2]. This approach showed narrow-band, small-FSR and non-flat-top spectral characteristics.

In this work, we demonstrate a silicon-on-insulator multimode Bragg gratings (MMBG) to achieve dual broadband filtering in the 1.5-1.6 μm spectral region, towards dual-band CWDM or LAN WDM applications. The MMBG is designed such that the self-coupling of odd modes and the inter-coupling of even modes create two well-defined pass bands in the drop port. The grating is formed using corrugated sidewalls similar to [3]. A simple asymmetric y-branch is used as mode converter and for measurement purposes.

2. Design and fabrication

The proposed design uses a Bragg grating in a multimode strip silicon waveguide. The three first TE modes are considered. Both the TE_0 and the TE_2 modes have symmetric electric field distributions, while the TE_1 mode's electric field shows antisymmetry, as shown in Figure 1 (a). According to the coupled-mode theory (CMT), a dielectric perturbation causes the coupling between two given modes having field distributions ϕ_m and ϕ_n. The coupling coefficient is given by the overlap integral between the fields and the perturbation profile [4]:

$$\kappa_{mn} = \frac{\omega}{4} \iint \varphi_m^*(x,y) \Delta\varepsilon(x,y) \varphi_n(x,y)\, dydx, \tag{1}$$

where $\Delta\varepsilon(x,y)$ describes the shape of the periodic perturbation imposed upon the waveguide. From Equation 1, it is possible to deduce what modes are allowed to couple into each other. In [5], an asymmetric Bragg grating allows the forward TE_0 mode to couple into the backward TE_1 mode. In our case, a symmetrical Bragg grating is used, i.e. $\Delta\varepsilon(x,y)$ is symmetric with respect to the longitudinal axis. This strictly allows for even-to-even mode coupling as well as self-coupling.

The phase-matching condition of the first-order Bragg reflection imposes $\beta_m - \beta_n = 2\pi/\Lambda$, where $\beta = 2\pi n_{eff}/\lambda$ is the propagation constant and Λ the grating pitch. The sign of β must account for the direction of propagation. In the case of self-coupling, $\beta_n = -\beta_m \equiv \beta$ and the Bragg reflection occurs at $\lambda_B = 2\Lambda n_{eff}$. When the coupling from a mode to another occurs, the Bragg reflection is located at $\lambda_B = 2\Lambda \bar{n}_{eff}$, i.e. the reflection wavelength is the arithmetic mean of the reflection wavelengths of each individual mode, as demonstrated in [6]. Figure 1 (b) shows the simulated effective indices and Bragg wavelengths based on a 320-nm pitch for all supported modes. The result of the coupling between TE_0 and TE_2 as a function of the waveguide width used is also shown. While the self-coupling of the different modes shows considerable spacing in terms of effective indices, for a waveguide width around 1.1 μm, the coupling of forward TE_0 into backward TE_2 yields a Bragg reflection close enough to that

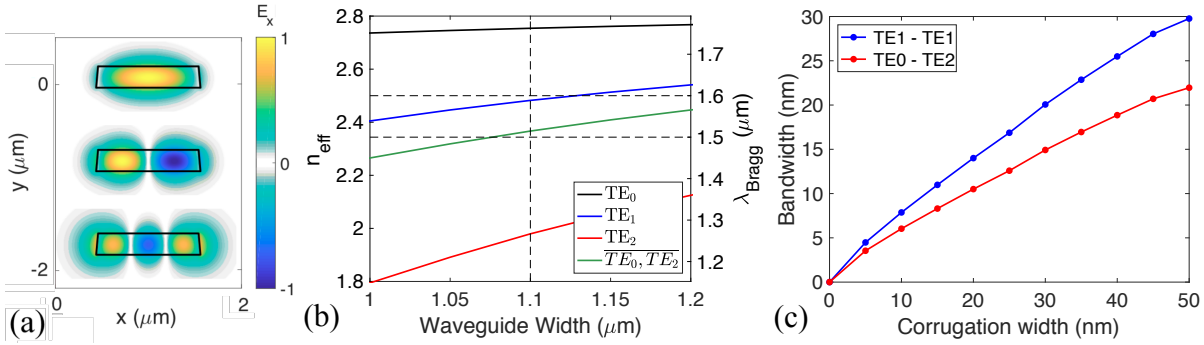

Fig. 1. (a) Simulated TE mode profiles. (b) Simulated mode-dependent effective indices and corresponding bragg wavelengths at 1550 nm as a function of waveguide width. (c) Reflection bandwidth as a function of corrugation width.

of the TE_1 self-coupling, such that both coupling conditions exhibit a reflection peak in the 1.5-1.6 μm spectral region. The principle of operation of this dual-band filter is hence based on the combined Bragg reflections of the TE_1 mode into itself and the contradirectional coupling between the TE_0 and TE_2 modes to obtain two distinct reflection bands.

Figure 1 (c) shows the simulated filter bandwidths as functions of corrugation width, based on the mode overlap (Equation 1). The bandwidths increase with the corrugations and so does the difference in bandwidths. This is due to the limited spatial overlap between the TE_0 and the TE_2 mode distributions, while the overlap between the TE_1 mode and itself is unsurprisingly higher. Hence, dual-band filtering with a wider most-right band is expected. The Bragg grating is also apodized according to the equation shown in Figure 2 (a) in order to avoid sidelobes in the reflection spectrum.

For measurement purposes, a y-branch was used. Y-branch responses depend on the considered modes. It was designed to be asymmetric such that both reflection bands have similar loss. By using branch widths of 600 and 475 nm, the simulated device showed both reflections bands having a total intrinsic loss of 12.5 dB due to the two-way passage through the device. Figure 2 shows the grating Gaussian apodization profile with a Gaussian parameter of 12, which was discretized for fabrication requirements. It also displays the scheme of the suggested device featuring the asymmetric y-branches placed on either side of the MMBG so as to allow add-drop-like operation.

The device was fabricated using Advanced Micro Foundry (AMF)'s 193-nm deep UV lithography process. An electron microscope image is displayed on Figure 2 (c), showing the corrugations near the center of the grating. The designed MMBG featured a 1.1-μm-wide multimode waveguide with 30-nm-wide sidewall corrugations and a 320-nm pitch. Due to lithography smoothing, the fabricated design actually displays a corrugation width of 10

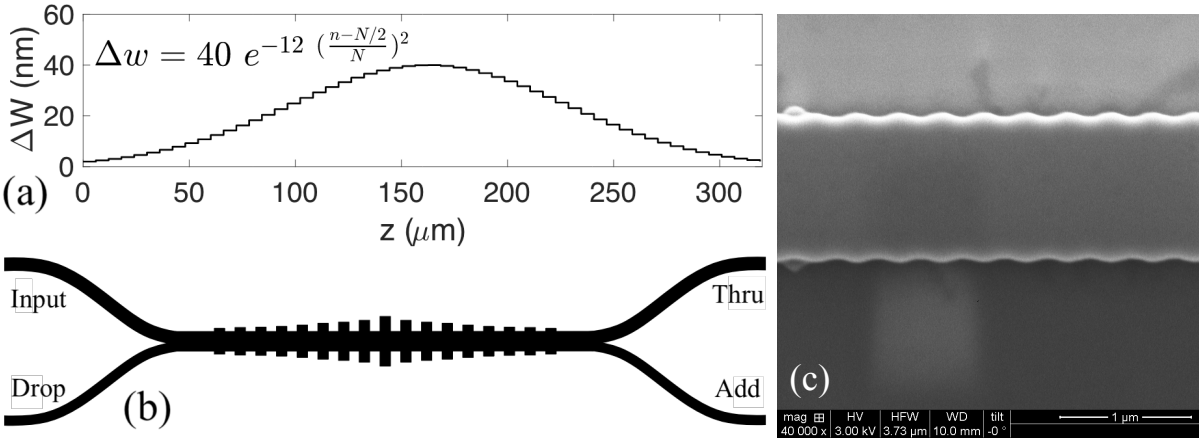

Fig. 2. (a) Apodization profile of the fabricated design. (b) Schematic of the fabricated device including apodized multimode Bragg grating and asymmetric y-branches used for characterization purposes. (c) Scanning electron microscope image of the fabricated device.

nm. This effect had been accounted for in the design as wider-than-needed corrugations were chosen.

3. Results

The fabricated device was tested using off-chip optical spectral analyzing and polarization controlling equipment. Figure 3 shows the measured transmissivity (thru-response) and reflectivity (drop-response) spectra. The drop-port response shows two well-defined reflection bands, centered at 1543 and 1585 nm, hence showing 42-nm band spacing. The reflection bandwidths are 4.4 and 7.5 nm, which agrees well with the simulation results shown on Figure 1 considering the as-fabricated 10-nm-wide sidewall corrugations. An out-of-band rejection ratio of 9.2 dB is also shown experimentally. This filter shows an experimental loss of 13 dB, which is considerable, although mainly caused by the asymmetric y-branch's intrinsic loss (12.5 dB simulated). This could be avoided by placing the device in a Mach-Zehnder configuration [7].

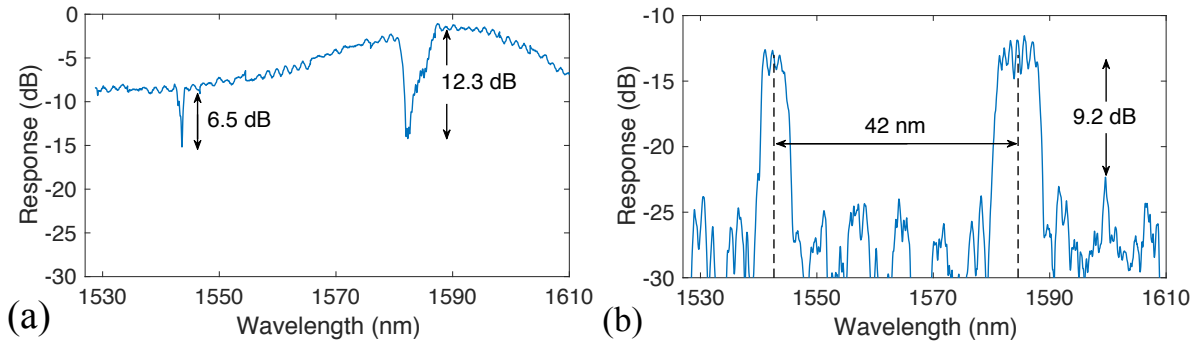

Fig. 3. Measured (a) thru-port and (b) drop-port responses.

4. Conclusion

We demonstrated dual-band optical filtering using multimode integrated Bragg gratings, achieving bandwidths of 4.4 and 7.5 nm and a 42-nm band separation in the 1.5-1.6 μm spectral region. This paves the way for compact and versatile dual-band WDM communication systems.

Acknowledgment

The authors would like to acknowledge the support from CMC Microsystems for the access to simulation and design software and the fabrication run. This research was funded by the Natural Sciences and Engineering Research Council of Canada (NSERC). Thanks to Philippe Jean for proof reading.

References

1. Iridan. Cwdm dual band, 2019.
2. Qingzhong Huang, Xinliang Zhang, Jinsong Xia, and Jinzhong Yu. Dual-band optical filter based on a single microdisk resonator. *Optics letters*, 36(23):4494–4496, 2011.
3. Jonathan St-Yves, Hadi Bahrami, Philippe Jean, Sophie LaRochelle, and Wei Shi. Widely bandwidth-tunable silicon filter with an unlimited free-spectral range. *Optics letters*, 40(23):5471–5474, 2015.
4. Amnon Yariv and Pocji Yeh. *Photonics: optical electronics in modern communications*. Oxford Univ., 2006.
5. Huiye Qiu, Jianfei Jiang, Ting Hu, Ping Yu, Jianyi Yang, Xiaoqing Jiang, and Hui Yu. Silicon add-drop filter based on multimode bragg sidewall gratings and adiabatic couplers. *Journal of Lightwave Technology*, 35(9):1705–1709, 2017.
6. Toru Mizunami, Tzvetanka V Djambova, Tsutomu Niiho, and Sanjay Gupta. Bragg gratings in multimode and few-mode optical fibers. *Journal of lightwave technology*, 18(2):230–235, 2000.
7. Dominique Charron and Wei Shi. O-band add-drop filter in bragg-grating-assisted mach-zehnder interferometers for cwdm. In *CLEO: Applications and Technology*, pages JTh2A–44. Optical Society of America, 2019.